Reciprocal interactions between CA1 pyramidal and axo-axonic cells control sharp wave-ripple events

Earl T. Gilbert[1†], Lianne M.F. Klaver[1†], Kaiser C. Arndt[1], Jongwoon Kim[2], Xiaoting Jia[2,3], Sam McKenzie [4*], Daniel Fine English[1*]

Affiliations

1. School of Neuroscience, Virginia Tech, Blacksburg, VA;

2. The Bradley Department of Electrical and Computer Engineering, Virginia Tech, Blacksburg, VA;

3. Department of Materials Science and Engineering, Virginia Tech, Blacksburg, VA;

4. Dept. of Neurosciences, University of New Mexico Health Sciences, Albuquerque, NM;

[†]These authors contributed equally to this work.

* Correspondence to neurodan83@vt.edu and samckenzie@salud.unm.edu

Abstract

Diverse sources of inhibition serve to modulate circuits and control cell assembly spiking across various timescales. For example, in hippocampus area CA1 the competition between inhibition and excitation organizes spike timing of pyramidal cells (PYR) in network events, including sharp wave-ripples (SPW-R). Specific cellular-synaptic sources of inhibition in SPW-R remain unclear,

as there are >20 types of GABAergic interneurons in CA1. Axo-axonic cells (AAC) are defined by their synaptic targeting of the axon initial segment of pyramidal cells, potently controlling spike output. The impact of AAC activity on SPW-R is controversial, due mainly to ambiguity of AAC identification. Here we monitored and manipulated opto-tagged AACs in behaving mice using silicon probe recordings. We found a large variability of AAC neurons, varying from enhanced to suppressed spiking during SPW-Rs, in contrast to the near-uniform excitation of other parvalbumin-expressing interneurons. AACs received convergent monosynaptic inputs from local pyramidal cell assemblies, which strongly influenced their participation in SPW-Rs. Optogenetic silencing of AACs increased power and duration of SPW-Rs, recruiting a greater number of PYR, suggesting AACs control SPW-R dynamics. We hypothesize that lateral inhibition by reciprocal PYR-AAC interactions thus supports the organization of cell assemblies in SPW-R.

Introduction

Inhibitory actions in the cortex and hippocampus are diverse, with >20 types of inhibitory interneurons existing along a spectrum, with varied genetic profiles, axonal targeting, and state dependent activity[1–5]. Given the complexity that emerges from the nonlinear dynamics of inhibitory interactions among these types, numerous functions have been attributed to both their global and specific operations[6–8]. Studying unique interneuron subtypes in the hippocampus has proven fundamental in understanding mechanisms underlying circuit function, including their role in various network oscillations, learning, place field tuning and replay of experience[3,4,9–13].

Axo-axonic cells (AACs) are anatomically distinct from other interneurons in two ways. First, only AACs target the axon initial segment of principal cells. Second, they do not target other interneuron types or each other, but instead, mutually interact with principal cells[14–16]. Despite the hypothesized importance of their distinct anatomical features, knowledge about AAC firing patterns in the behaving animal and their role in circuit control is limited[3,14,17,18]. Spiking activity of AACs has been mainly examined in connection with hippocampal sharp wave ripples (SPW-R), a network event critical in memory selection and consolidation, but their specific role has remained controversial[3,17–20].

Leveraging the recent availability of the Unc-5b-Cre mouse-line[14], which enables genetic access to AACs, we conducted *in vivo* silicon probe recordings to characterize the spiking activity of CA1 AACs in SPW-R. We report that participation of AACs in SPW-R falls along a continuum, driven by diverse interactions with CA1 pyramidal cells. Using optogenetic inhibition of AACs we found that AACs exhibit control over CA1 circuitry, most strongly during SPW-R. SPW-R that occurred during AAC-OFF epochs were of longer duration and higher power, though unchanged

in frequency. Similarly, during AAC-OFF SPW-R, CA1 pyramidal cell recruitment was enhanced, suggesting that the magnitude of circuit activation during SPW-R, and potentially cell assembly selection, is controlled by AACs. These results demonstrate a critical role for AACs in CA1 SPW-R.

Results

To characterize the activity of AACs, we recorded LFP and ensemble spiking in the hippocampal CA1 region of awake mice expressing excitatory or inhibitory opsins in AACs (**Fig 1A**). Selective opsin expression was achieved by injecting AAV2/5 encoding Cre-dependent opsins into the CA1 layer of adult Unc5B-CreER mice[14], allowing us to opto-tag AACs. AACs were identified by activation or inactivation (ChR2 or Arch expressing AACs; **Fig 1B**). We identified cellular-synaptic properties of 43 AACs and examined how their reciprocal interactions with CA1 pyramidal cells organize circuit activity during SPW-R.

Characteristics of CA1 axo-axonic cells

We quantified physiological metrics of AACs (n=43 AACs, n=7 animals, 17 sessions). The somata of AACs were observed mostly in or close to the pyramidal layer (**Fig 1C,** μ=4.33µm relative to center of pyramidal layer, σ= 212.4) in agreement with previous studies[14,17,19]. Spike width was variable, (**Fig 1D**) with a trough to peak latency range of 0.18-0.68ms (**Fig 1F**, μ=0.35ms, σ=0.14)**,** as were spike autocorrelations (**Fig 1E**). Mean firing rates were observed from 0.18-32.47hz (**Fig 1G,** μ=11.14hz, σ=8.62), with inter-spike intervals (ISI) ranging between 0.41ms to 285.71ms (**Fig 1H,** μ=45.45ms, σ=55.95). A small group of AACs showed transiently fast spiking ("bursting"), while the population had an observed range of 0.0036-0.6621 (burst

index is fraction of spikes with less than 6-ms ISI[21]; **Fig 1I,** μ=0.1747, σ= 0.1906). This unexpected spectrum of physiology is interesting as it stands in contrast to the notion that AACs are monolithic, rather they exhibit significant intra-class variability as suggested in Varga et al., 2014[17].

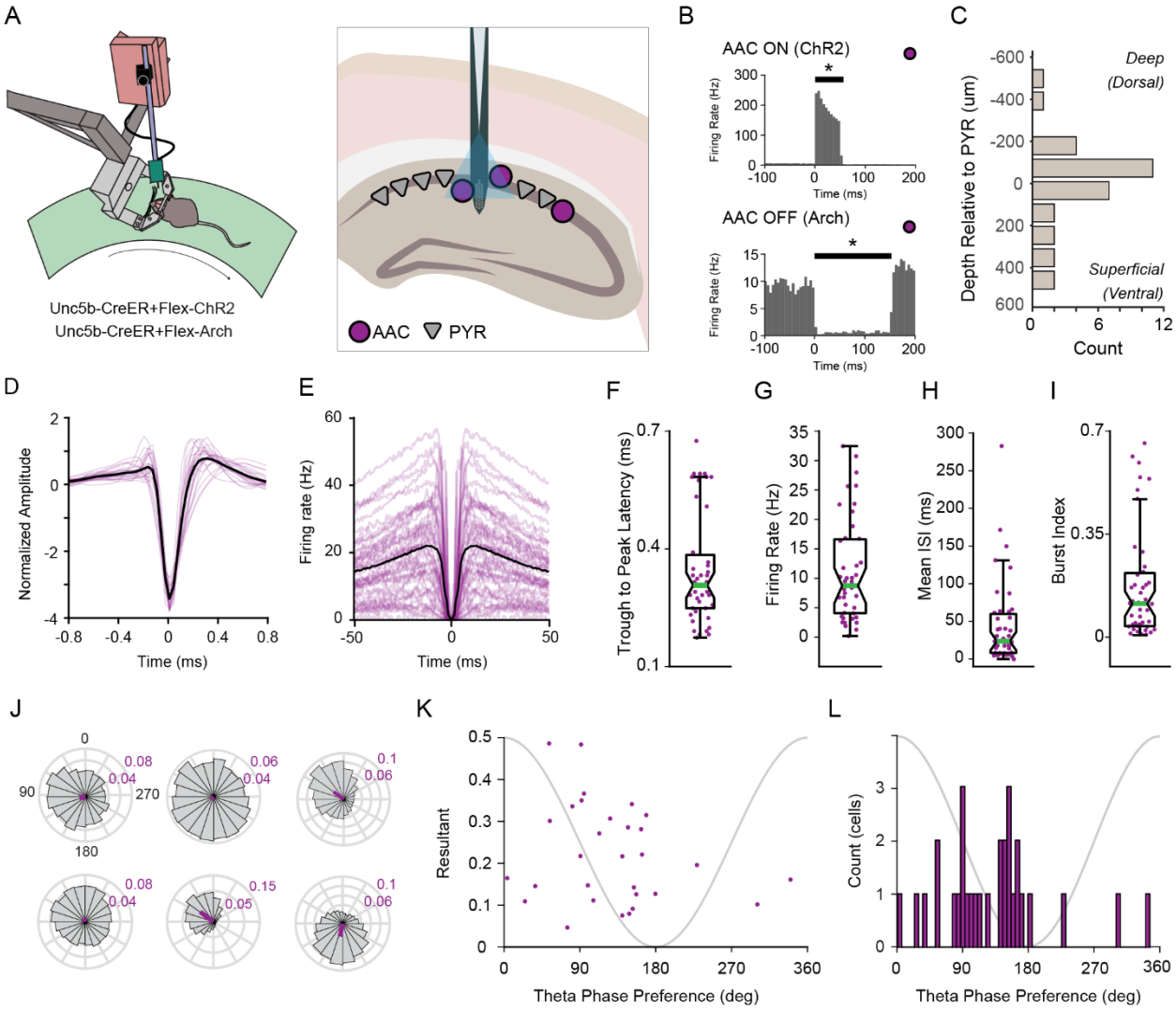

Figure 1: Firing characteristics of axo-axonic cells

A.) Cartoon of experimental set-up. Head-fixed mice run on a disc with an acutely implanted silicon probe in CA1 of the hippocampus. A sharpened optic fiber, glued to the probe, is used to stimulate axo-axonic cells.

B.) Example peri-stimulus time histograms of two units' responses to ChR2 (top) or Arch (bottom) activation. Putative interneurons with significant responses to the stimulus were identified as opto-tagged AACs.

C.) Soma position of AACs relative to the pyramidal layer of CA1 (n=32 cells, μ=6.0μm, σ=215.6)

D.) Average (black) and individual (purple) mean extracellular spike waveforms (n=43 cells)

E.) Average (black) and individual (purple) spike autocorrelations (n=43 cells)

F.) Trough to peak latency of extracellular waveforms. (n=43 cells, μ=0.35, σ=0.14)

G.) Average firing rate (Hz) of AACs (n=43 cells, μ=11.14Hz, σ=8.62)

H.) AAC inter-spike-interval (ms, n=43 cells, μ=45.45ms, σ=55.95)

I.) Distribution of burst index (n=43 cells, μ=0.1747, σ=0.1906)

J.) Example polar plots of spike entrainment to the theta oscillation of 6 AACs from one recording session.

K.) Theta phase modulation versus phase preference of significantly theta modulated AACs (n=30 cells, Circular-Linear correlation, rho=0.7872, p=9.1922e-05)

L.) Distribution of significantly theta modulated AACs phase preferences (n=30 cells)

Axo-axonic cells preferentially spike at the descending phase of the local theta oscillation

Prior reports have shown strong modulation of AAC spiking by phase of the ongoing theta rhythm[3,17]. Here we report in the largest to date collection of AACs (n=43). We found that many AACs were strongly theta modulated, similar to many CA1 interneurons. Theta phase preference of six AACs from a single recording session are shown in **Fig 1J**, demonstrating the observed variability is not due to inter-animal differences. The majority of AACs exhibit significant theta phase modulation (30/32, **Supplementary Table 1,** Rayleigh z test). Theta phase preference and phase modulation were correlated (**Fig 1K,** rho=0.7872, p=9.1922e-5, Circular-linear correlation coefficient), and most AACs spikes were distributed on the descending phase of theta(**Fig 1L**). The average theta phase preference for the population was 110.28°, while the most theta modulated

108 AAC exhibited a phase preference of 91.04°. AACs as a population are highly theta modulated
109 cells, with a phase preference for the descending phase of the oscillation[3,17,18].

110 **Axo-axonic cells are activated in SPW-R**

111 The participation of AACs in CA1 SPW-R is critical to understanding their role in the CA1
112 circuit, though there are mixed reports as to their level of participation[3,14,17–20]. Ripple-associated
113 spiking activity of 43 AACs (**Fig 2A,** n=43 cells, n=595-16,058, μ=5,666.4 SPW-R per recording
114 session), revealed diverse participation across the population. On average AACs have significantly
115 increased firing rate during SPW-R (**Fig 2B**, Left: n=43 cells, baseline x̃=6.13hz, SPW-R
116 x̃=10.69hz, p=3.5132e-4, Wilcoxon signed-rank test). Interestingly, out of the 40 AACs that
117 changed their firing rate (ZETA[22]), 27 cells increased and 13 cells decreased their activity (**Fig 2B**,
118 Right), which stands in contrast to other types of interneurons with a more uniform response, such
119 as PV+ cells (**Fig S1,** 43/46 cells showed increased activity). AACs demonstrated strong ripple
120 phase modulation with most cells firing on the ascending phase of the ripple oscillation (100-
121 250Hz, **Fig 2C,** $\boldsymbol{\theta}_{\mu}$=255.02 degrees), similar to previous reports for PV+ cells.

122 Single cell ripple modulation values (SPW-R firing rate gain) ranged from .61-3.01 (**Fig**
123 **2D,** μ=1.24, σ=0.46). The average number of spikes in SPW-R ranged from 1.02-4.73 (**Fig 2E**,
124 μ=2.02, σ=1.02), while inter-spike intervals of AACs in SPW-R ranged from 9.1-37.2ms,
125 approximating a range of 1-5 cycles of the oscillation (**Fig 2F**, μ=20.3ms, σ=7.0). Additionally,
126 because SPW-R information content systematically varies from the beginning to end of each event,
127 we calculated the average time of the first spike from the peak of the SPW-R, which ranged from
128 -21.7-42.0ms (**Fig 2G**, μ=-7.5ms, σ=0.0064), suggesting AACs influence activity throughout the
129 SPW-R event. Together these findings demonstrate that AAC activity in SPW-Rs is variable,

however most AACs increase their activity in SPW-R events.

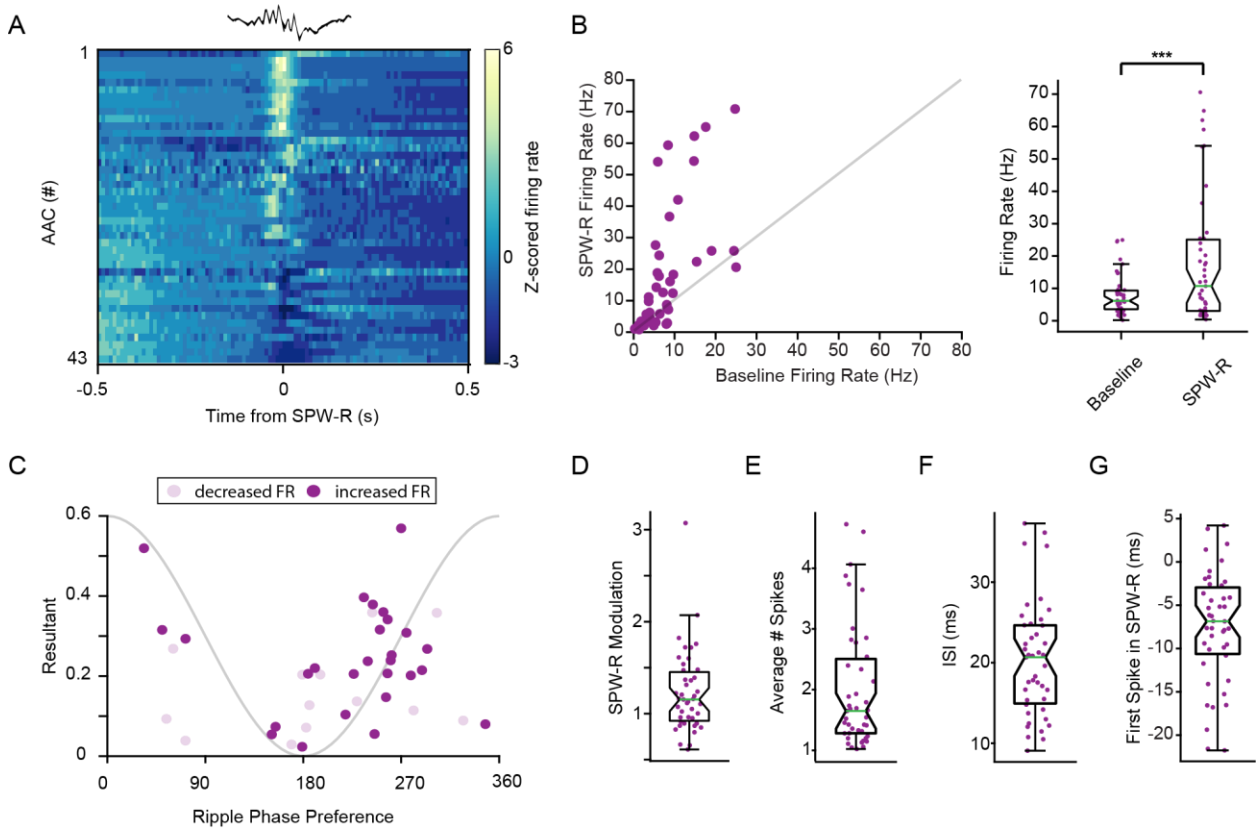

Figure 2: AACs firing is modulated by sharp wave-ripples

A.) Peri-event time histogram of AAC z-scored firing rate centered on SPW-R peak (n=43 cells, 1,495-16,058 SPW-R events, μ=5,666.4 events)

B.) Left: Scatter plot of baseline firing rate versus firing rate during SPW-R of each AAC. (n=43). Right: Firing rate (Hz) in baseline and within SPW-R. (n=43 cells, baseline x̃=6.13hz, SPW-R x̃=10.69hz, p=3.5132e-4, Wilcoxon signed rank test)

C.) Ripple wave phase modulation versus phase preference of significantly SPW-R modulated AACs (n=40 cells)

D.) SPW-R modulation of significantly modulated AACs (n=40 cells, μ=1.24, σ= 0.46)

E.) Average number of spikes fired in SPW-R events (n=43 cells, μ=2.02, σ= 1.02)

F.) Inter-spike-interval during SPW-R (n=43 cells, μ=20.3ms, σ= 7.0)

G.) Average delay to first spike in SPW-R from the peak of SPW-R (n=43 cells, μ=-7.5ms, σ=6.4)

CA1 pyramidal neurons control the participation of axo-axonic cells in SPW-R

144 To determine if local excitation is a mechanism by which AAC activity is modulated in
145 SPW-R, we quantified excitatory synaptic inputs from local CA1 PYR. Such monosynaptic
146 connections were identified using a validated monosynaptic inference method[23,24] (based on cross-
147 correlations of putatively-classified pyramidal cells and AACs). For AACs with at least one
148 presynaptic PYR, we calculated the average SPW-R modulation of the presynaptic inputs.
149 Example SPW-R cross-correlations (**Fig 3A**) illustrate both strongly and weakly modulated AACs
150 and their partners (note that an AAC with a large peak in the cross-correlation at the time of SPW-
151 R has partners that also show a large peak, **Fig 3A, top**). AAC ripple modulation correlated with
152 that of its inputs, such that AACs that received synaptic drive from ripple modulated PYR were
153 themselves strongly ripple modulated. (**Fig 3B,** r=0.6923, p=1.3325e-4, Spearman's Rank
154 Correlation; correlation with randomly selected non-presynaptic partner control, r=0.1915
155 p=0.3574, Spearman's Rank Correlation; see Fig S2 for correlations with other physiological
156 metrics.). We found further evidence that the CA1 PYR modulate AAC activity in SPW-R when
157 examining other metrics. We quantified the correlation between spiking activity and power in the
158 ripple frequency band as well as the magnitude of phase modulation. There was a significant
159 relationship between spike rate power correlation of presynaptic PYR and AACs (**Fig 3C**,
160 r=0.4619, p=0.0185, Spearman's Rank Correlation), as well as ripple phase modulation between
161 paired cells (**Fig 3D** r=0.5015 p=0.0099, Spearman's Rank Correlation). Given the relationship
162 between presynaptic and AAC activity, we investigated the relationship between strength of
163 presynaptic connections and AAC participation in SPW-R. Both AAC SPW-R modulation and
164 time to first spike were related to spike transmission probability. Stronger spike transmission
165 probability was associated with higher ripple modulation (**Fig 3E,** r=0.5508, p=0.0041,
166 Spearman's Rank Correlation), and a shorter delay between first spike and SPW-R peak (**Fig 3F,**

r=-0.7039, p= 9.2163e-5, Spearman's Rank Correlation). These results suggest that excitation from CA1 PYR controls AAC activity during SPW-R.

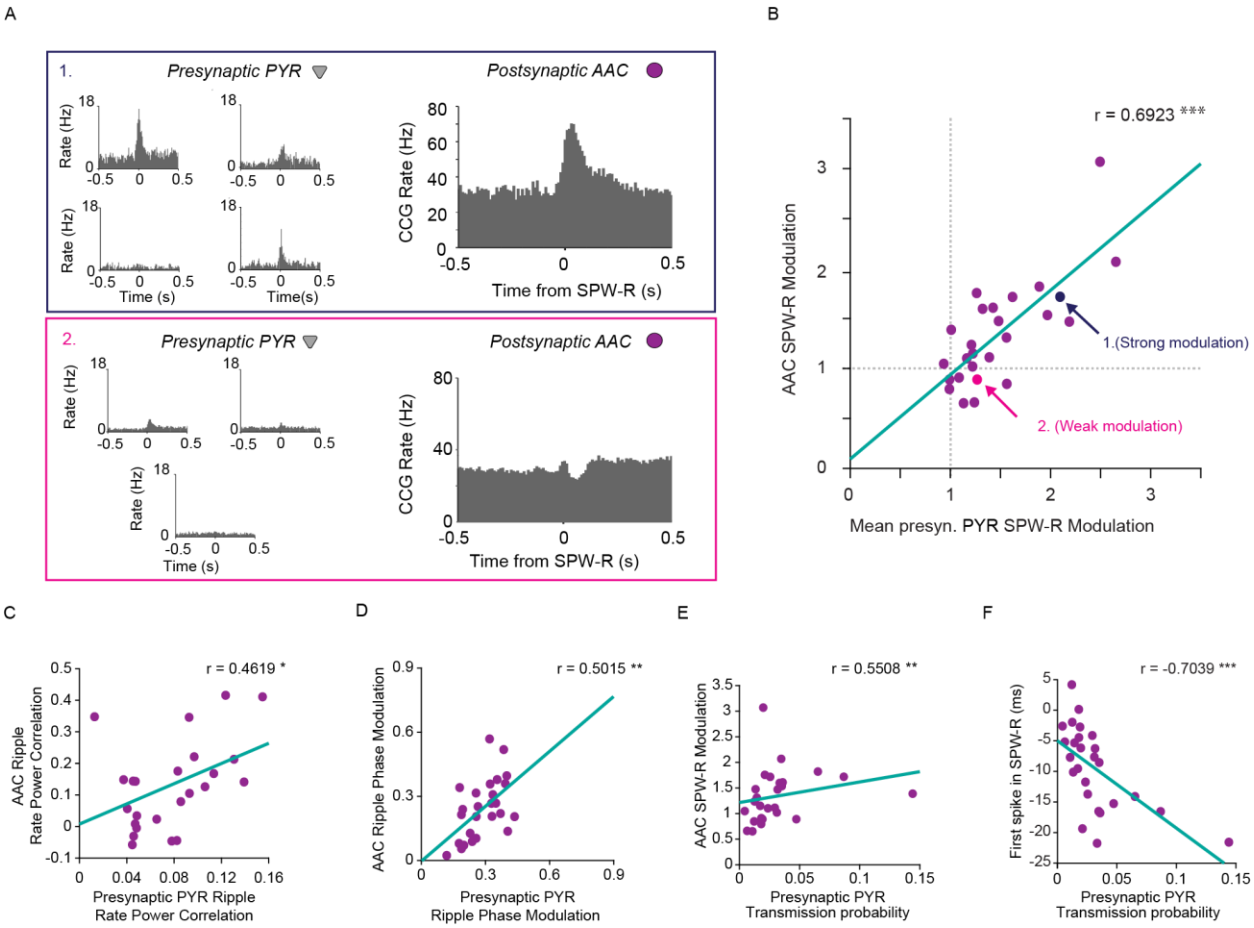

Figure 3: Local presynaptic pyramidal cells contribute to spiking of AACs in SPW-R

A.) Top: SPW-R cross-correlograms between 4 pyramidal cells presynaptically (prePYR) connected to a strongly ripple-activated AAC (right). Bottom: Example SPW-R cross-correlograms between 3 pyramidal cells presynaptically connected to a of a weakly ripple modulated AAC.

B.) Correlation between average SPW-R modulation of presynaptic PYR and their monosynaptically connected AACs (n=25 AACs, n=1-8 prePYR, r=0.6923, p=1.3325e-4, Spearman's Rank Correlation). Arrows point to the example sets in A.

C.) Correlation between average rate power correlations of spike to ripple frequency (100-250Hz) power of presynaptic partners and AACs (n=25 AACs, n=1-8 prePYR, r=0.4619, p=0.0185, Spearman's Rank Correlation)

D.) Correlation between average ripple (100-250Hz) phase modulation of presynaptic partners and AACs (n=25 AACs, n=1-8 prePYR, r=0.5015 p=0.0099, Spearman's Rank Correlation)

E.) Correlation between average PYR-AAC spike transmission probability and SPW-R modulation of AACs (n=25 AACs, n=1-8 prePYR, r=0.5508, p=0.0041, Spearman's Rank Correlation)

F.) Correlation between average PYR-AAC spike transmission probability and AAC average delay to first spike in SPW-R from peak (n=25 AACs, n=1-8 prePYR, r=-0.7039, p= 9.2163e-5, Spearman's Rank Correlation)

AACs control network-wide spiking activity and SPW-R dynamics

We found that AACs robustly participate in SPW-R, though whether they influence the generation of SPW-R in the network remains unknown. To address this question, we optogenetically inhibited local AACs expressing archaerhodopsin (Arch). Silencing AACs increased power in the ripple band (100-250hz, **Fig 4A,B**, Bottom: n=5 sessions, 4 mice. n=843-1,936 300ms stims. p=0.0020, Paired T-test), as well as power in the 300-500Hz band, which reflects population spiking activity (300-500hz, **Fig 4A,B**, Top: n=5 sessions, 4 mice. n=843-1,936 300ms stims. P=3.0224e-04, Paired T-test). We then detected SPW-R and examined properties of such events occurring either in or out of AAC inhibition epochs. Subtraction of baseline ripple PSDs from AAC-OFF ripple PSDs reveal increased power of the ripple frequency at the time of these events. (**Fig 4C**, n=5 sessions, 4 mice. n=1,495-12,364 baseline ripples, n= 64-335 stim ripples), as did event durations (**Fig 4E**, n=5 sessions, 4 mice. n=37,032 baseline ripples, n= 1,024 stim ripples. p=0.0072, Wilcoxon rank sum-test), and peak amplitude (**Fig 4F**, n=5 sessions, 4 mice. n=37,032 baseline ripples, n=1,024 stim ripples. p=2.0593e-06, Wilcoxon rank sum test), while ripple frequency was not affected (**Fig 4D**, n=5 sessions, 4 mice. n=37,032 baseline ripples, n=1,024 stim ripples. p=0.8675, Wilcoxon rank-sum test). This suggests that AACs control content and magnitude of SPW-R while other cell types may pace the rhythm (likely basket cells[25]). These data reveal an important role for AACs in controlling SPW-R dynamics at the network level.

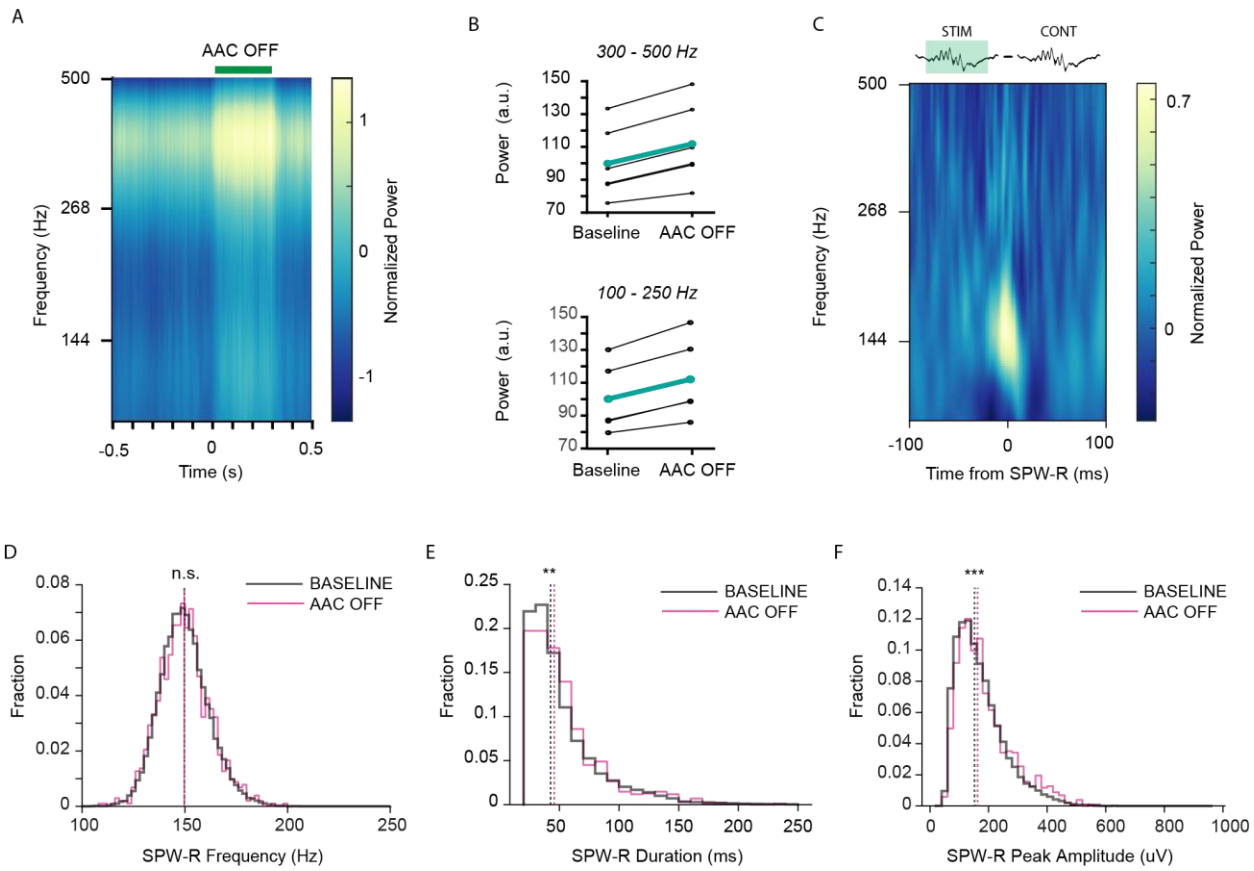

Figure 4: Axo-axonic cells affect SPW-R dynamics

A.) Mean peri-stimulus power spectral density (PSD) of AAC-Arch activation (n=5 sessions, 4 mice. n=843-1,936 300ms stims)

B.) Average power of PSD in A comparing baseline (-300ms:0ms) to stimulation (0ms:300ms) in the spike band (top, 300-500Hz n=5 sessions, 4 mice. n=843-1,936 300ms stims. p=3.0224e-04, Paired T-test) and the SPW-R band (bottom, 100-250Hz. n= 5 sessions, 4 mice. 843-1,936 300ms stims. p=0.0020, Paired T-test)

C.) Average SPW-R event PSD of baseline events subtracted from AAC-OFF events (n=5 sessions, 4 mice. n=1,495-12,364 baseline ripples, n=64-335 AAC-OFF ripples.)

D.) Distribution of frequency of AAC-OFF SPW-R events compared to baseline control (n=5 sessions, 4 mice. n=37,032 baseline ripples, n= 1,024 AAC-OFF ripples. p=0.8675, Wilcoxon rank sum test.)

E.) Distribution of duration of AAC-OFF SPW-R events compared to baseline control (n=5 sessions, 4 mice. n=37,032 baseline ripples, n= 1,024 AAC-OFF ripples. p=0.0072, Wilcoxon rank sum test.)

F.) Distribution of peak amplitude of AAC-OFF SPW-R events compared to baseline control (n=5 sessions, 4 mice. n=37,032 baseline ripples, n= 1,024 AAC-OFF ripples. p=2.0593e-06, Wilcoxon rank sum test.)

217 **AACs control pyramidal cell participation in SPW-R**

218 Pyramidal cells are reliably depolarized during SPW-R, and competition between excitatory and
219 inhibitory inputs compete to determine spiking at the single cell level[12]. Given our findings that
220 most AACs are active in SPW-R, and inhibiting them alters SPW-R dynamics, we next
221 investigated the effects of silencing AACs on PYR spiking. We first looked at the effects of
222 manipulating AAC activity in all states. AAC activation inhibited PYR firing, while AAC
223 silencing resulted in PYR disinhibition, revealed by changes in their firing rates. (**Fig 5A**, Left,
224 ChR2: n=11 sessions, 4 mice. n=1,063-4,459 100ms stims, n=180 PYR, Right, Arch: n=5 sessions,
225 4 mice. n=843-1,936 300ms stims, n=207 PYR). These results demonstrate that AACs tonically
226 inhibit PYR. Next, we sought to investigate how AAC inhibition shapes PYR activity selectively
227 during SPW-R by comparing baseline ripples to ripples that occurred during periods where AACs
228 were silenced. We quantified the fraction of PYR that participated in AAC-OFF SPW-R compared
229 to baseline. In AAC-OFF SPW-R, we observed a significant increase in PYR participation (**Fig**
230 **5B**, Left: AAC: n=5 sessions, 4 mice. n=31-55, total: 194 PYR. n=1,495-12,364, total: 37,032
231 Baseline SPW-R. n=51-287, total: 868 AAC-OFF SPW-R. p=5.2716e-16, Wilcoxon rank-sum
232 test). Superficial and deep CA1 PYR receive different patterns of inhibition[26,27], thus we quantified
233 this effect separately for each subgroup of pyramidal population. In AAC-OFF SPW-R, the
234 fraction of both superficial and deep PYR participation increased (**Fig S3**, Right: Top, AAC,
235 n=1,495-12,364, total: 37,032 Baseline SPW-R. n=51-287, total: 868 AAC-OFF SPW-R. n=11-
236 32, total: 125 Deep cells, n=5-33, total: 69 Superficial cells. Deep: p=2.4645e-13, Wilcoxon rank-
237 sum test. Superficial: p=6.5141e-06, Wilcoxon rank-sum test.). Given that cell assemblies
238 constructed from unique sets of PYR enable the encoding of separate experiences by SPW-R[28–31]
239 we examined SPW-R associated PYR activity at an individual cell level. On average, PYR

240 exhibited a higher count of spikes in AAC-OFF SPW-R (**Fig 5C**, n=5 sessions, 4 mice. n=194
241 PYR, n=1,495-12,364 Baseline SPW-R. n=51-287 AAC-OFF SPW-R. p=6.1155e-08, Wilcoxon
242 signed-rank test). Similarly, pyramidal cell SPW-R firing rate gain was significantly higher when
243 AACs were silenced (**Fig 5D**, n=5 sessions, 4 mice. n=194 PYR, n=1,495-12,364 Baseline SPW-
244 R. n=51-287 AAC-OFF SPW-R. p=2.4569e-08, Wilcoxon signed-rank test). Increased firing rate
245 was naturally reflected in decreased inter-spike interval in AAC-OFF SPW-R. (**Fig 5E**, n=5
246 sessions, 4 mice. n=194 PYR, n=1,495-12,364 Baseline SPW-R. n=51-287 AAC-OFF SPW-R.
247 p=6.9834e-05, Wilcoxon signed-rank test.) Further, AACs participated in a higher fraction of total
248 AAC-OFF SPW-R than baseline SPW-R. (**Fig 5F**, n=5 sessions, 4 mice. n=194 PYR, n=1,495-
249 12,364 Baseline SPW-R. n=51-287 AAC-OFF SPW-R. p=1.8104e-11, Wilcoxon signed-rank
250 test). These results demonstrate AACs control the participation of pyramidal cells in SPW-R
251 events, likely contributing to functions such as replay.

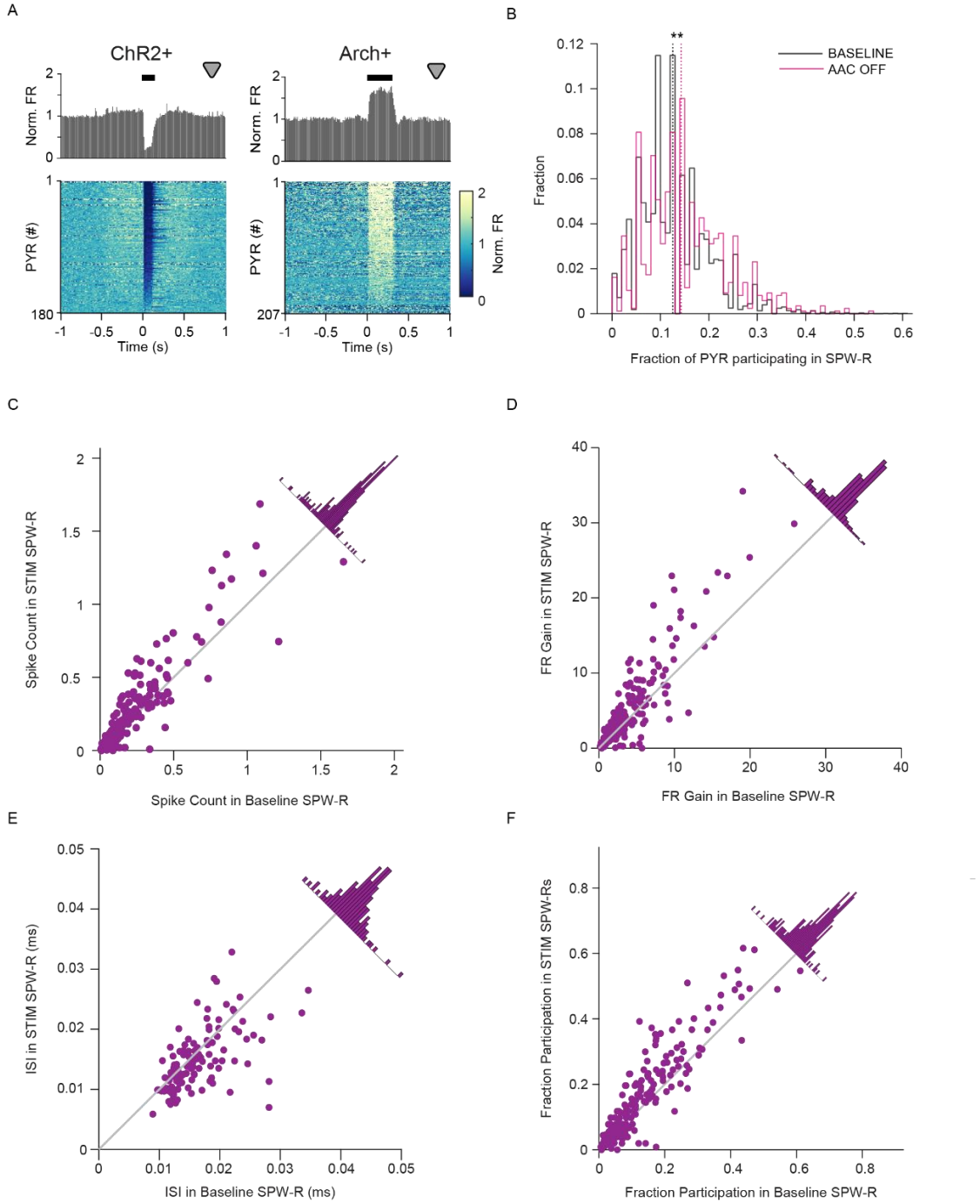

Figure 5: AACs control pyramidal cell participation during SPW-R

A.) Peri-stimulus time histograms of PYR firing rate in response to stimulation of interneurons in a subset of sessions with matched stim durations. (**Left**, ChR2: n=11 sessions, 4 mice. n=1,063-4,459 100ms stims, n=180 PYR, **Right**, Arch: n=5 sessions, 4 mice. n=843-1,936 300ms stims, n=207 PYR)

B.) Distribution of fraction of PYR participating in baseline and AAC-OFF SPW-R. (n=5 sessions, 4 mice. n=31-55, total: 194 PYR. n=1,495-12,364, total: 37,032 Baseline SPW-R. n=51-287, total: 868 AAC-OFF SPW-R. p=5.2716e-16, Wilcoxon rank-sum test.)

C.) Scatter plot of individual PYR mean spike count in baseline SPW-R versus count in AAC-OFF SPW-R. Gray: Unity Line. Distribution of distances from unity line on diagonal. (n=5 sessions, 4 mice. n=194 PYR, n=1,495-12,364 Baseline SPW-R. n=51-287 AAC-OFF SPW-R. p=6.1155e-08, Wilcoxon signed-rank test)

D.) Scatter plot of individual PYR firing rate gain in baseline SPW-R versus firing rate gain in AAC-OFF SPW-R. Gray: Unity Line. Distribution of distances from unity line on diagonal. n=5 sessions, 4 mice. n=194 PYR, n=1,495-12,364 Baseline SPW-R. n=51-287 AAC-OFF SPW-R. p=2.4569e-08, Wilcoxon signed-rank test)

E.) Scatter plot of individual PYR inter-spike interval in baseline SPW-R versus inter-spike interval in AAC-OFF SPW-R. Gray: Unity Line. Distribution of distances from unity line on diagonal. (n=5 sessions, 4 mice. n=122 PYR, n=1,495-12,364 Baseline SPW-R. n=51-287 AAC-OFF SPW-R. p=6.9834e-05, Wilcoxon signed-rank test.)

F.) Scatter plot of fraction of baseline SPW-R in which individual PYR participated versus participation in AAC-OFF SPW-R. Gray: Unity Line. Distribution of distances from unity line on diagonal. (n=5 sessions, 4 mice. n=194 PYR, n=1,495-12,364 Baseline SPW-R. n=51-287 AAC-OFF SPW-R. p=1.8104e-11, Wilcoxon signed-rank test.)

Discussion

Glutamatergic excitation and GABAergic inhibition compete to control PYR participation in SPW-R[25]. In each SPW-R, only a minority of PYR spike even though Vm is depolarized above spike threshold for 10's of milliseconds, due to dynamically balanced GABAergic inhibition. Inhibition thus plays a critical role in enabling competition-based selection and expression of PYR assemblies. Identifying the source(s) of this inhibition is critical to understanding the CA1 circuit, and likely arises from axo-somatic targeting cells such as basket cells and AACs. Here we identify novel mechanisms by which AACs participate in and control CA1 SPW-R. Notably, these findings strongly suggest that reciprocal interactions between excitatory PYR and inhibitory AACs organize cell assembly construction and overall network activity during SPW-R. This places AACs in a critical position in determining the content of CA1 information delivered to neocortex.

283 **Recruitment of AACs to sharp wave-ripples is explained by monosynaptic inputs from CA1**
284 **PYR**

285 CA1 interneuron spiking is controlled both by afferent inputs (e.g., CA3) and excitation
286 and inhibition from local PYR and INT, respectively[32–34]. To determine the activity of AACs and
287 PYR during SPW-R at single-spike resolution, we used silicon probes to obtain CA1 ensemble
288 recordings and opto-tagged AACs. As a population, AAC activity is significantly increased during
289 SPW-R, with a minority of cells exhibiting decreased activity, emphasizing the importance of
290 considering intra-class variability in studying cell types[17] (**Fig 2A,B)**. In agreement with these
291 findings, up- and down-modulated AACs have been previously described in studies using both
292 juxta-cellular electrophysiology[26] and calcium imaging[14,19]. To better understand the driver of
293 AAC spiking in SPW-R, we examined their physiology and excitatory inputs from CA1 PYR.
294 Individual AAC activity in SPW-R is strongly correlated with the activity of presynaptic partners
295 and the strength of these connections (**Fig 3)**, suggesting that the local circuit can control AAC
296 activity independently of afferent input. An important future question is if the propensity for AACs
297 to participate in SPW-R is consistent across experiences and/or throughout the lifespan of the
298 animal[35]. Such plasticity could be supported both by changes in excitatory inputs we identified as
299 well as inhibition from local interneurons[36]. Longitudinal recording of single AACs would be
300 required to answer these questions.

301 **AACs control network activation and PYR spiking in sharp wave-ripples**

302 Silencing AACs led to increased power in both the spiking band and SPW-R band (**Fig**
303 **4A,B**), SPW-R events that occurred during AAC silencing were of longer duration, and had higher
304 power and peak amplitude (**Fig 4C,F,G**). Interestingly AAC silencing did not alter SPW-R
305 frequency. These data support a model in which AACs robustly control PYR recruitment, while

306 other interneurons such as PV+ cells may be more important for synchronizing PYR populations
307 at ripple frequency[25].

308 PYR activity in SPW-R was affected significantly by silencing AACs. Inhibition of AACs
309 increased the number of participating PYR (**Fig 5B)** and produced increased average spike count,
310 firing rate gain and decreased inter-spike intervals (**Fig 5C,D,E)**. Additionally, PYR participated
311 in a greater fraction of AAC-OFF epochs than during control SPW-R, suggesting AACs function
312 to select which PYR are allowed to participate in each event. Our findings that during SPW-R,
313 silencing AACs disinhibits PYR, and that PYR drive AAC spiking, suggests lateral inhibition is
314 instantiated by reciprocal interactions between pyramidal cells and AACs. These results support
315 the general hypothesis that individual interneurons serve unique functions in CA1 circuit
316 computations, and that this mechanism supports the construction of and competition between cell
317 assemblies. Our experiments demonstrate this specifically for the understudied AAC interneuron
318 family.

319 # Methods

320 All protocols and experiments using animals were approved by the Virginia Tech (Blacksburg,
321 VA, USA) Institutional Animal Care and Use Committee (IACUC). The Unc5b-CreER mice were
322 obtained from Z. Josh Huang under a fully executed MTA, and either maintained on a homozygous
323 C57BL/6J background or were bred with FVBN/J wild-type mice to generate heterozygous mice.
324 Male and female adult mice (>12 weeks) were used in all experiments.

325 **AAV Injection**

326 Mice are induced and maintained at a surgical plane of anesthesia with isoflurane while mounted
327 in a stereotaxic frame. Hair is removed and scalp is disinfected. Bupivicaine is injected once
328 under the scalp before revealing skull. A < 0.2 mm burr hole is made above area CA1 of the
329 hippocampus in both hemispheres. (mm from bregma: −1.8, lateral: +/-1.5). Glass pipette
330 containing AAV5-EF1a-DIO-hChR2 (H134R)-EYFP or AAV5-EF1a-DIO-eArch3.0-EYFP
331 (UNC Gene Therapy Center – Vector Core) is lowered into CA1 using stereotaxic coordinates.
332 100nL of AAV (titer: 3.8-5.2x10^{12} GC/mL) is injected into tissue (1nLs^{-1}) using a nanoliter
333 injector (WPI: MICRO2T & 504127). Following infusion, the glass pipette is left to rest for 5
334 minutes before slowly removing from the brain. The scalp is then closed with Vetbond (3M).

335 **Tamoxifen injections**

336 Mice were injected intraperitoneally with tamoxifen (100 mg/kg) dissolved in corn oil at 20
337 mg/ml on days 5,7, and 9 following AAV injection.

338 **Head-bar Implantation**

339 Mice are induced and maintained at a surgical plane of anesthesia with isoflurane while mounted
340 in a stereotaxic mount. Bupivicaine is injected under the scalp before it is removed. The skull is
341 cleaned with 3% hydrogen peroxide, followed by an application of dental adhesive Optibond
342 (Kerr Dental). A small burr hole is made above cerebellum, and a stainless-steel ground wire is
343 inserted between the skull and the brain, parallel to the brain surface, then the wire is affixed to
344 the skull with sterile dental acrylic. A headplate is positioned parallel to the skull above lambda,
345 and is permanently fixed in place.

346 **Craniotomy**

347 One day before recording, mice are induced and maintained at a surgical plane of anesthesia with
348 isoflurane while mounted in the stereotaxic mount. A <1.0 mm burr hole is made above the
349 hippocampus and the dura is removed. Kwik-cast (World Precision Instruments) is applied to the
350 burr hole, with dental acrylic applied on top, to protect the craniotomy until recording.

351 ***In Vivo* recording**

352 Unc5b-CreER mice were obtained from the lab of Z. Josh Huang under full MTA. All animals
353 used in experiments were homozygous Unc5b-CreER or hybrid Unc5b-CreER x FVB/NJ (JAX
354 #001800) mice. Additionally, PV-Cre mice were acquired from the Jackson Laboratory (Jax
355 #017320). During the time of experiments, mice were between the ages of 16–30 weeks old.
356 Mice of both sexes were used in all experiments. Mice, trained and habituated to head-fixed
357 navigation, are placed in the head fixation apparatus, and a silicone probe (Poly3, Neuronexus, or
358 P1, Cambridge Neurotech, with optic fiber attached, or 4x8 uLED, Neurolight technologies), is
359 lowered through the craniotomy into the brain until SPW-R are observed and left in place for 30-

360 45 minutes until tissue is relaxed. The neural signals were amplified, digitized and recorded with
361 RHD2000 system (Intan Technologies LLC).

362 **Optical Stimulation**

363 Optical pulses were delivered through a sharpened optic fiber connected to a Thorlabs laser
364 diode driver and laser diode or optical pulses are delivered through LEDs in a 4x8 uLED probe
365 (Neurolight Technologies).

366 **Data collection**

367 Unc5b-CreER ChR2, Arch, and PV+ data was collected for this study. A selection of PV+ data
368 was used with permission from the Buzsaki Data Repository[24,37].

369 **Data analysis**

370 Data analysis was conducted in Matlab (Mathworks) and custom scripts were used to analyze the
371 extracellular and spike data. Spike sorting was performed using Kilosort1[38] with custom semi-
372 automated reclustering[39] followed by manual curation using Phy. Cell Explorer[40] was used to
373 characterize neuron properties including cell position, autocorrelation, wave form characteristics,
374 firing rate characteristics, putative monosynaptic connections (followed by manual refinement)
375 and SPW-R modulation. The Buzcode repository was used to calculate cross correlations and for
376 SPW-R detection. The HippoCookBook repository and Circular Statistics Toolbox (Mathworks)
377 were used to quantify oscillation phase preference and phase modulation. Rate power correlation
378 was calculated by correlating spike trains with power in the SPW-R band (100-250Hz). Opto-
379 tagged AACs were identified using CellExplorer to classify putative cell type, and Zenith of Event-
380 based Time-locked Anomalies (ZETA[22]) to determine significance of the response to stimulation.

381 Further, opto-tagged AACs were manually refined through observation of peri-stimulation time
382 histogram to optical stimulation. Significance of SPW-R modulation was determined using
383 CellExplorer and ZETA. For detection of SPW-R characteristics in and out of stimulation (Fig 4),
384 SPW-R were classified as having the peak of the event within stimulation times. For detection of
385 spikes from cells in SPW-R events (Fig 5), only SPW-R that had the entire duration within a
386 stimulation pulse were considered INT-OFF SPW-R.

387 Acknowledgements

388 The research in this report was supported by grants to from the National Institute of Neurological
389 Disorders and Stroke (NINDS) R01NS131858 (DFE and SM), The Whitehall Foundation (DFE)
390 and The Simons Foundation (DFE). We would like to thank Gyorgy Buzsaki and Ivan Soltesz for
391 comments on previous versions of this manuscript, Zachary Saccomano for assistance with
392 analytical approaches, and Z. Josh Huang for providing the Unc5b-CreER mouse line.

393 Author Contributions

394 E.G., L.M.F.K., S.M., and D.F.E. designed the study. E.G., S.M., L.M.F.K and D.F.E. conducted
395 experiments. E.G., L.M.F.K., K.A., J.K., S.M., and D.F.E. conducted data analysis. All authors
396 contributed to the writing of the manuscript.

397 Supplemental Information

398 **Table 1: Quantification of AAC characteristics**

AAC ID	Position	Trough to Peak	AB Ratio	Firing Rate	ISI	Burst Index	Theta Phase Preference	Theta Phase Modulation	Theta, Rayleigh's Z p Value	Baseline Firing Rate	SPW-R Firing Rate	SPW-R ZETA p value	SPW-R Phase Preference	SPW-R Phase Modulation	SPW-R, Rayleigh's Z p Value	SPW-R Modulation	SPW-R Avg # Spikes	SPW-R ISI	SPW-R Time to First Spike	Average Partner SPW-R Modulation	SPW-R Rate Power Correlation	Average Partner SPW-R Rate Power Correlation	Average Partner SPW-R Phase modulation	Average Partner Transmission Probability
1 6	-129.7036144	0.358333333	0.517676112	2.45659825	4.194044457	0.033225337	1.867729722	0.346354849	1.71521E-83	1.750663184	2.170900445	0.001289698	4.881621794	0.211475012	5.20365E-11	0.958106638	1.058951965	0.034704938	0.032934473	NaN	0.013634235	NaN	NaN	NaN
1 8	-4.703614369	0.275	0.305668564	2.446166462	8.631851532	0.174530493	1.726930991	0.339490704	8.89021E-36	1.043222309	1.683007355	6.33823E-05	1.104397112	0.30039568	1.80137E-16	1.158013544	1.04735376	0.021223529	0.033319355	NaN	0.029189153	NaN	NaN	NaN
2 4	512.1489619	0.533333333	0.097159056	5.139507864	5.499541705	0.007582459	5.708889376	0.17902593	1.35914E-19	2.417160847	1.633270435	1.11133E-07	0.94812035	0.094026679	0.050264097	0.94739819	1.109215017	0.021405625	0.039035665	NaN	-0.072199777	NaN	NaN	NaN
2 5	87.14896194	0.191666667	0.54831025	18.87011398	285.7142857	0.662133636	2.371827833	0.333284352	0	5.791307611	53.79951269	0.000112	4.251868485	0.379022531	0	1.819361063	3.645897174	0.010500103	0.014182297	1.888138414	0.415729553	0.123539113	0.354789621	0.065258536
3 5	-25.60401344	0.183333333	0.194945823	7.482463992	14.78560867	0.045526704	2.087895876	0.232658033	1.48826E-72	5.67776301	18.37416202	1.11022E-16	4.765203544	0.560273572	0	1.53468781	1.694171956	0.021631255	0.023465404	1.968933028	0.167668641	0.113525584	0.352727363	0.035244249
3 7	74.39598656	0.366666667	0.264573488	22.55592314	173.4104046	0.595111928	2.623041071	0.217453163	9.18888-132	8.293771928	59.07768716	1.49046E-06	4.450624742	0.548560261	0	2.067827298	3.737133308	0.010762887	0.011673284	2.652707289	0.410882801	0.154759735	0.418604288	0.034773089
3 8	-25.60401344	0.283333333	0.361983125	12.13836676	151.5151515	0.616551106	2.844417697	0.109714752	1.09056E-08	3.55190151	10.68905611	0.014419146	4.80287125	0.3196632	3.90432E-79	1.468817204	1.682758621	0.019582155	0.027783492	2.18779909	0.141057494	0.139117151	0.36567121	0.031747672
3 11	-25.60401344	0.575	-0.19096249	0.184767322	0.409081612	0.031736872	1.816963416	0.166217826	0.245379686	0.154847766	0.563240661	0.007008132	2.798512297	0.09442027	0.453497438	1.188405797	1.022727273	0.099003333	0.032744144	NaN	0.031249398	NaN	NaN	NaN
4 2	NaN	0.266666667	0.457453513	6.785950396	27.8551532	0.069269166	5.530717009	0.071497156	0.000575626	6.129939103	23.97403685	8.70548E-12	4.439691769	0.185828927	4.77594E-14	3.069230769	2.853502555	0.017085546	0.023171166	2.494117647	0.125912026	0.106115066	0.276558405	0.019792517
4 3	NaN	0.25	0.402280627	30.7620074	54.64400674	0.237560637	0.068434637	0.185512896	1.71138-135	24.70584109	70.61348409	1.11022E-16	4.559324929	0.240974677	8.42969E-68	1.717687075	4.725043783	0.011463736	0.011939734	2.095393839	0.220934212	0.096978903	0.253314081	0.086790568
4 8	NaN	0.35	0.161179724	1.892672009	8.844339623	0.039565511	0.531094164	0.114519973	0.013002151	1.693957823	2.903668342	0.18742396	4.131517249	0.360760056	4.52153E-07	1.21875	1.2	0.027854386	0.041036201	NaN	-0.003283557	NaN	NaN	NaN
5 4	-47.54009572	0.283333333	0.269913118	12.67177049	88.49557522	0.470837092	2.121958039	0.168875194	2.17869E-54	5.229621193	27.24345744	7.85683E-10	4.339380487	0.301730858	0	1.474925478	2.398322851	0.017517841	0.023244022	1.481502178	0.213036612	0.130629778	0.255303069	0.013428863
6_15	-71.88211722	0.2	0.47285508	25.67061703	66.96428571	0.182362214	5.595005329	0.15063681	6.68421E-88	24.42501048	25.42476978	0.912590877	5.042183007	0.170812366	8.55917E-32	0.998702325	2.335947712	0.013715275	0.016271619	NaN	0.098002173	NaN	NaN	NaN
7 10	-551.9782049	0.333333333	-0.284402809	11.76207356	24.89626556	0.089469268	5.511597517	0.011421037	0.735842003	8.133070633	7.064594595	1.85807E-07	0.052994522	0.074430007	0.000544454	0.864506307	1.455954195	0.028514175	0.030097726	NaN	0.010604089	NaN	NaN	NaN
7 13	-551.9782049	0.308333333	0.412948571	16.84425652	38.61003861	0.087818982	2.182225057	0.271340833	3.31E-213	10.72748316	41.68002749	8.73897E-19	4.770534327	0.407065586	0	1.608092618	2.822411788	0.016604248	0.015935669	1.426153524	0.142829366	0.037282396	0.216518416	0.035979842
7 14	-101.9782049	0.25	0.111877315	25.75198226	64.65517241	0.285845685	2.196315462	0.268971774	0	14.72120805	61.97520202	3.53067E-16	4.274165149	0.074767825	2.44969E-50	1.755015045	3.876452665	0.012195787	0.01173142	1.262543843	0.175469041	0.085123162	0.204813082	0.021169673
7 15	-201.9782049	0.233333333	0.517718026	21.37774802	122.9508197	0.539949968	2.06146421	0.23372045	9.1627E-138	8.636595698	36.53188273	3.2885E-06	4.990515745	0.077567219	8.38338E-19	1.715941614	2.775590551	0.015338548	0.018252615	1.620601956	0.143852532	0.045360063	0.236350603	0.025583957
8 4	NaN	0.316666667	0.067058094	8.724201607	18.35985312	0.113817807	0.259837805	0.261175231	2.8813E-110	7.05431549	12.14893144	0.004279917	5.054302891	0.244629157	9.47644E-14	1.236137667	1.544642857	0.020809654	0.038052935	1.210409696	0.059985615	0.048495546	0.355788491	0.012620691
8 12	NaN	0.391666667	-0.232147968	9.506980777	18.4729064	0.018830546	5.69048259	0.237489135	1.25364E-64	7.982563514	8.240008989	0.07613908	4.376582793	0.149586267	0.00080717	0.956066946	1.523809524	0.02063782	0.0260848	NaN	-0.025099403	NaN	NaN	NaN
9 17	NaN	0.308333333	-0.337506428	32.47436212	132.7433628	0.545012485	6.204750192	0.3312694	1.4548E-279	18.95076083	25.42200173	0.000110828	5.063976354	0.201932258	9.07138E-44	1.111791106	3.007592191	0.012446335	0.032433648	1.388756643	0.078825124	0.085663691	0.166688966	0.02944254
10 9	-41.8014161	0.216666667	-0.250867822	10.03181969	31.38075314	0.147509415	0.967135751	0.111970864	0.035915235	6.101737224	17.35504334	1.27428E-07	6.014774394	0.089167882	3.29359E-05	1.309667674	1.793103448	0.022279644	0.028759075	1.560493827	0.104946285	0.092990942	0.172336079	0.014462396
11 17	NaN	0.283333333	0.220256024	10.25190052	63.69426752	0.30537331	3.898249212	0.128238937	0.013771222	5.4154702	13.80965923	1.56936E-08	2.147817503	0.022673294	0.421898163	1.357886905	2.136764706	0.020924105	0.029861765	NaN	0.067516617	NaN	NaN	NaN
12 1	15.26160312	0.175	0.754407868	22.66992890	55.86592179	0.219504068	1.203989269	0.282461922	0	17.52374621	64.87982846	6.27797E-18	4.612985995	0.295802547	0	1.597203617	4.600922442	0.012043253	0.012838795	1.321709429	0.345891181	0.092692643	0.093398023	0.033465091
12 12	-84.73839688	0.191666667	-0.005408642	27.9957558	62.5	0.209951188	0.465572816	0.293772017	0	24.94192369	20.19803549	0.000063102	6.050706444	0.091953567	6.53071E-39	0.889472961	2.541675641	0.016653142	0.022450952	1.267535029	-0.004776817	0.048264746	0.24254947	0.047355233
12 13	-184.7383969	0.291666667	0.204065391	6.740515812	90.36144579	0.501687791	0.322814744	0.247043456	7.86302E-40	3.895313103	3.871532223	0.001774545	4.944550538	0.147469659	6.9273E-20	1.365449628	1.649890591	0.020923644	0.036847108	NaN	0.02993116	NaN	NaN	NaN
13 6	NaN	0.333333333	-0.078376253	10.56569744	31.41361257	0.109425664	1.478432739	0.36787162	2.0957E-284	9.600664784	17.87057108	3.76706E-11	4.509919637	0.026479139	0.274119029	1.1015625	1.929896907	0.025318334	0.027426009	1.164215686	0.143046001	0.047330223	0.216500806	0.023708522
13 17	70.45559405	0.341666667	0.313840844	0.038347828	7.473841555	0.014487276	2.093411833	0.286920207	1.59268E-55	3.551128273	9.34566949	3.76987E-08	2.96529369	0.209122162	2.99965E-19	1.150071124	1.42503639	0.034405594	0.031246737	1.224770642	0.056501895	0.040423527	0.224482104	0.017259399
13_18	24.72272165	0.591666667	0.017083734	4.131766586	8.685581954	0.022241372	1.554138637	0.387757236	1.0554E-99	3.791018286	5.765867591	5.22064E-07	9.923143583	0.188805127	4.63687E-10	1.070080863	1.350396476	0.057190444	0.037554982	NaN	0.073163837	NaN	NaN	NaN
13 37	-25.27727835	0.258333333	0.28008317	16.72122681	41.15226337	0.118874525	1.847959018	0.272054347	3.5038E-195	14.63611796	54.03114332	2.55668E-17	3.467494796	0.178761119	5.70965E-79	1.387262984	4.063173008	0.014173572	0.014059636	1.008474576	0.347682764	0.012776277	0.258548994	0.144067991
14 8	-108.6963636	0.316666667	-0.631916275	3.354312894	5.976069417	0.003550175	0.112502018	0.530538901	0	3.15136838	3.216817366	3.17319E-08	0.662148956	0.523767809	2.43626E-169	1.047012506	1.130212766	0.027143137	0.031514622	0.934136771	-0.030732978	0.045819838	0.390605287	0.004427417
14 13	-208.6963636	0.225	0.619235267	3.20666587	6.570302234	0.04857609	1.459317861	0.354049433	0	2.976799322	5.195833291	5.66214E-15	4.211503761	0.241863655	1.28891E-55	1.155615697	1.198993851	0.024568633	0.026395143	NaN	0.023570795	NaN	NaN	NaN
14 22	-108.6963636	0.508333333	-0.533956963	8.751068208	15.52795031	0.044086858	1.656699009	0.22614228	1.5848E-302	8.366991616	6.712199489	5.24875E-20	4.034155874	0.143775084	2.19355E-25	0.908845482	1.283464567	0.0257776	0.029121148	1.087061841	-0.044433825	0.082375608	0.412173133	0.018217142
15 15	NaN	0.183333333	0.43901236	9.435509971	18.10500905	0.124466996	1.263446075	0.244821265	0	8.780652968	15.65872611	7.77156E-16	5.012117948	0.146861517	2.11594E-45	1.127366609	1.6625	0.02459972	0.024447947	NaN	0.055295311	NaN	NaN	NaN
15 17	NaN	0.325	0.924707825	5.512566823	40.10695187	0.065869687	1.421560619	0.338267948	1.0282E-224	5.275471288	2.662114255	1.08389E-07	4.818452269	0.367914591	1.12329E-49	1.202654867	1.423076923	0.023028099	0.032946154	NaN	0.052826815	NaN	NaN	NaN
18 10	-10.91994241	0.241666667	0.563974861	16.37899523	41.09589041	0.165307536	2.581436593	0.308727958	0	15.29893879	21.9576955	2.1023E-09	4.569026434	0.084177181	6.1915E-56	1.019718467	1.886541943	0.018281548	0.022522085	1.22157558	0.00826389	0.047097124	0.29901424	0.031143245
18 11	314.0800576	0.583333333	-0.286067228	8.140799773	23.16602317	0.011341428	0.595853835	0.508278981	0	7.882451096	2.104923038	4.72105E-21	5.578711147	0.146398913	1.51187E-16	0.652305825	1.280626781	0.017571066	0.0196077	1.131960557	-0.04614779	0.078009695	0.053274527	0.010835228
18 13	289.0800576	0.675	-0.441062863	4.981701355	9.140767824	0.165817697	0.005532983	0.108710535	4.39527E-40	4.79511036	1.633129943	1.35166E-22	3.397078869	0.215840538	2.20836E-27	0.660620188	1.254513274	0.015473082	0.024872535	1.239699055	-0.057832882	0.044687286	0.199093008	0.006579539
18 23	439.0800576	0.591666667	-0.18357031	8.388652194	24.23263328	0.039664533	0.598265409	0.298510682	1.0778E-264	8.097688564	2.437402539	5.12872E-09	3.394339604	0.054212106	0.003159392	0.86530497	1.735	0.014785941	0.019443739	NaN	-0.079460159	NaN	NaN	NaN
18 29	139.0800576	0.591666667	-0.058069902	2.524861122	5.279366476	0.111766639	2.117999457	0.079193234	7.419466-15	2.401342891	1.640154158	3.58189E-09	3.563390356	0.388920222	1.15421E-92	0.824099723	1.147420147	0.017803148	0.028681188	NaN	-0.044575561	NaN	NaN	NaN
18 41	314.0800576	0.583333333	-0.336534067	1.259344447	7.211538461	0.174958814	1.305195038	0.1236463	9.39301E-14	1.20635434	0.364008468	2.85179E-17	3.270716663	0.21258738	1.18509E-06	0.607050731	1.358078603	0.012975203	0.020549353	NaN	-0.026302518	NaN	NaN	NaN
19 16	225.4251052	0.333333333	0.283499301	6.99447281	24.48979592	0.03867567	1.444067116	0.502827358	0	6.235516369	5.314767463	5.30676E-09	1.119304133	0.267847784	1.661E-105	0.845923824	1.316019033	0.024772689	0.033417519	1.563571755	0.023147123	0.065302297	0.361461634	0.012220651
19 22	0.42510516 5	0.291666667	0.466671554	10.07481128	23.41820375	0.021565315	2.308700362	0.280383126	0	9.473672818	11.93300607	1.04435E-06	3.415267702	0.213302757	2.44198-149	0.889102286	1.412969283	0.022350398	0.024249077	0.991571526	-0.017829569	-0.000377515	0.371348104	0.018159144

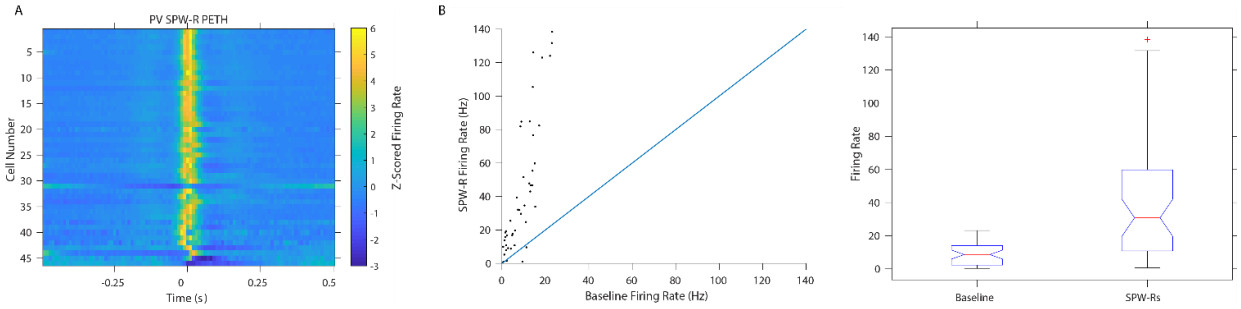

Figure S1: PV+ cells increase their firing rate during SPW-R.

A.) Peri-event time histogram of PV z-scored firing rate centered on SPW-R peak (n=46 cells, n=6 animals, 11 sessions. 2,031-10,960 SPW-R events, μ= 6,725.6 events)

B.) Left: Firing rate (Hz) in baseline and within SPW-R. (n=46 cells, n=6 animals, 11 sessions. baseline x̃= 8.63Hz, SPW-R x̃= 30.82Hz, p=3.0939e-4, Wilcoxon signed rank test) Right: Distribution of delta firing rate in and out of SPW-R (n=46 cells).

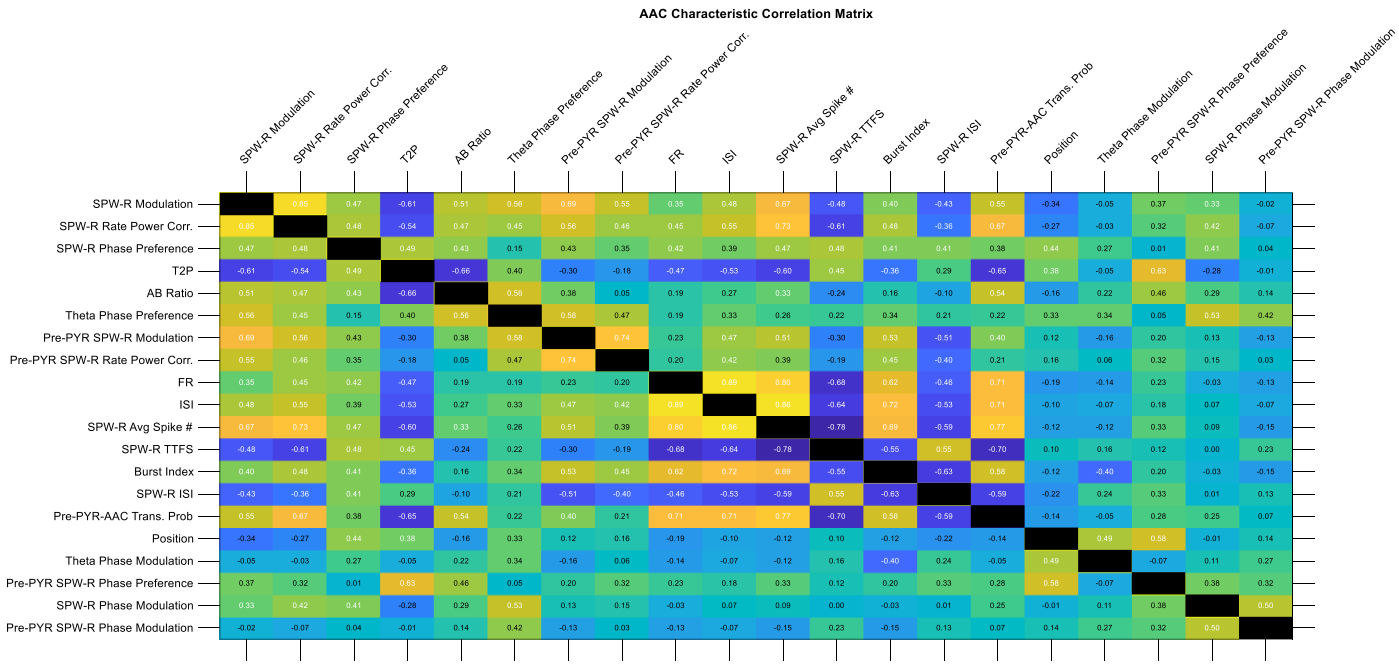

Figure S2: Correlation Matrix of AAC characteristics.

Clustered correlation matrix of AAC characteristics including SPW-R metrics of presynaptic PYRs. Significant correlations are labeled in white text ($p<.05$, Spearman's Rho, Circular-Linear Correlation Coefficient, and Circular-Circular Correlation Coefficient, respectively).

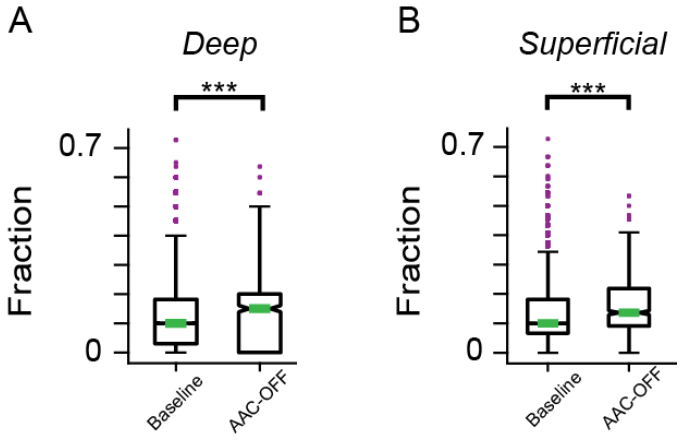

Figure S3: Both the fraction of deep and superficial PYRs participating is increased in AAC-OFF SPW-R

PYR cell participation separated by soma depth (n=1,495-12,364, total: 37,032 Control SPW-R. n=51-287, total: 868 AAC-OFF SPW-R.)

A.) Fraction of Deep PYR participating in SPW-R (n=11-32, total: 125 Deep cells, p= 2.4645e-13, Wilcoxon rank-sum test).

B.) Fraction of Superficial PYR participating in SPW-R (n=5-33, total: 69 Superficial cells. p= 6.5141e-06, Wilcoxon rank-sum test).

References

1. Bugeon, S. *et al.* A transcriptomic axis predicts state modulation of cortical interneurons. *Nature* **607**, 330–338 (2022).
2. Harris, K. D. *et al.* Classes and continua of hippocampal CA1 inhibitory neurons revealed by single-cell transcriptomics. *PLOS Biology* **16**, e2006387 (2018).

429 3. Klausberger, T. *et al.* Brain-state- and cell-type-specific firing of hippocampal
430 interneurons in vivo. *Nature* **421**, 844–848 (2003).
431 4. Klausberger, T. & Somogyi, P. Neuronal Diversity and Temporal Dynamics:
432 The Unity of Hippocampal Circuit Operations. *Science* **321**, 53–57 (2008).
433 5. Lapray, D. *et al.* Behavior-dependent specialization of identified hippocampal
434 interneurons. *Nat Neurosci* **15**, 1265–1271 (2012).
435 6. Buzsáki, G. & Chrobak, J. J. Temporal structure in spatially organized neuronal
436 ensembles: a role for interneuronal networks. *Current Opinion in Neurobiology*
437 **5**, 504–510 (1995).
438 7. Cobb, S. R., Buhl, E. H., Halasy, K., Paulsen, O. & Somogyi, P.
439 Synchronization of neuronal activity in hippocampus by individual GABAergic
440 interneurons. *Nature* **378**, 75–78 (1995).
441 8. Tremblay, R., Lee, S. & Rudy, B. GABAergic Interneurons in the Neocortex:
442 From Cellular Properties to Circuits. *Neuron* **91**, 260–292 (2016).
443 9. Klausberger, T. *et al.* Spike timing of dendrite-targeting bistratified cells during
444 hippocampal network oscillations in vivo. *Nat Neurosci* **7**, 41–47 (2004).
445 10. Klausberger, T. *et al.* Complementary roles of cholecystokinin- and
446 parvalbumin-expressing GABAergic neurons in hippocampal network
447 oscillations. *J Neurosci* **25**, 9782–9793 (2005).

11. Royer, S. *et al.* Control of timing, rate and bursts of hippocampal place cells by dendritic and somatic inhibition. *Nat Neurosci* **15**, 769–775 (2012).
12. English, D. F. *et al.* Excitation and inhibition compete to control spiking during hippocampal ripples: intracellular study in behaving mice. *The Journal of Neuroscience* **34**, 16509–16517 (2014).
13. Dudok, B. *et al.* Alternating sources of perisomatic inhibition during behavior. *Neuron* **109**, 997-1012.e9 (2021).
14. Dudok, B. *et al.* Recruitment and inhibitory action of hippocampal axo-axonic cells during behavior. *Neuron* **109**, 3838-3850.e8 (2021).
15. Li, X.-G., Somogyi, P., Tepper, J. M. & Buzs□ki, G. Axonal and dendritic arborization of an intracellularly labeled chandelier cell in the CA1 region of rat hippocampus. *Exp Brain Res* **90**, (1992).
16. Somogyi, P. A specific 'axo-axonal' interneuron in the visual cortex of the rat. *Brain Res* **136**, 345–350 (1977).
17. Varga, C. *et al.* Functional fission of parvalbumin interneuron classes during fast network events. *Elife* **3**, (2014).
18. Viney, T. J. *et al.* Network state-dependent inhibition of identified hippocampal CA3 axo-axonic cells in vivo. *Nat Neurosci* **16**, 1802–1811 (2013).

466 19. Geiller, T. *et al.* Large-Scale 3D Two-Photon Imaging of Molecularly
467 Identified CA1 Interneuron Dynamics in Behaving Mice. *Neuron* **108**, 968-
468 983.e9 (2020).
469 20. Vancura, B., Geiller, T., Grosmark, A., Zhao, V. & Losonczy, A. Inhibitory
470 control of sharp-wave ripple duration during learning in hippocampal recurrent
471 networks. *Nat Neurosci* **26**, 788–797 (2023).
472 21. Mizuseki, K., Royer, S., Diba, K. & Buzsáki, G. Activity dynamics and
473 behavioral correlates of CA3 and CA1 hippocampal pyramidal neurons.
474 *Hippocampus* **22**, 1659–1680 (2012).
475 22. Montijn, J. S. *et al.* A parameter-free statistical test for neuronal
476 responsiveness. *eLife* **10**, e71969 (2021).
477 23. Barthó, P. *et al.* Characterization of Neocortical Principal Cells and
478 Interneurons by Network Interactions and Extracellular Features. *Journal of*
479 *Neurophysiology* **92**, 600–608 (2004).
480 24. English, D. F. *et al.* Pyramidal Cell-Interneuron Circuit Architecture and
481 Dynamics in Hippocampal Networks. *Neuron* **96**, 505-520.e7 (2017).
482 25. Stark, E. *et al.* Pyramidal cell-interneuron interactions underlie hippocampal
483 ripple oscillations. *Neuron* **83**, 467–480 (2014).
484 26. Lee, S.-H. *et al.* Parvalbumin-positive basket cells differentiate among
485 hippocampal pyramidal cells. *Neuron* **82**, 1129–1144 (2014).

27. Mizuseki, K., Diba, K., Pastalkova, E. & Buzsáki, G. Hippocampal CA1 pyramidal cells form functionally distinct sublayers. *Nature Neuroscience* **14**, 1174–1181 (2011).
28. Buzsáki, G. Two-stage model of memory trace formation: a role for 'noisy' brain states. *Neuroscience* **31**, 551–570 (1989).
29. Buzsáki, G., Horváth, Z., Urioste, R., Hetke, J. & Wise, K. High-frequency network oscillation in the hippocampus. *Science* **256**, 1025–1027 (1992).
30. Nádasdy, Z., Hirase, H., Czurkó, A., Csicsvari, J. & Buzsáki, G. Replay and time compression of recurring spike sequences in the hippocampus. *The Journal of Neuroscience* **19**, 9497–9507 (1999).
31. O'Neill, J., Senior, T. & Csicsvari, J. Place-Selective Firing of CA1 Pyramidal Cells during Sharp Wave/Ripple Network Patterns in Exploratory Behavior. *Neuron* **49**, 143–155 (2006).
32. Topolnik, L. & Tamboli, S. The role of inhibitory circuits in hippocampal memory processing. *Nat Rev Neurosci* **23**, 476–492 (2022).
33. Andersen, P., Eccles, J. C. & LøYNING, Y. Hippocampus of the Brain: Recurrent Inhibition in the Hippocampus with Identification of the Inhibitory Cell and its Synapses. *Nature* **198**, 540–542 (1963).
34. McKenzie, S. Inhibition shapes the organization of hippocampal representations. *Hippocampus* **28**, 659–671 (2018).

35. Lee, J. S., Briguglio, J. J., Cohen, J. D., Romani, S. & Lee, A. K. The Statistical Structure of the Hippocampal Code for Space as a Function of Time, Context, and Value. *Cell* **183**, 620-635.e22 (2020).
36. Szabo, G. G. *et al.* Ripple-selective GABAergic projection cells in the hippocampus. *Neuron* **110**, 1959-1977.e9 (2022).
37. Petersen, P. C., Hernandez, M. & Buzsáki, G. The Buzsaki Lab Databank - Public electrophysiological datasets from awake animals. Zenodo https://doi.org/10.5281/zenodo.4307883 (2020).
38. Pachitariu, M., Steinmetz, N., Kadir, S., Carandini, M. & Kenneth D., H. *Kilosort: Realtime Spike-Sorting for Extracellular Electrophysiology with Hundreds of Channels*. http://biorxiv.org/lookup/doi/10.1101/061481 (2016) doi:10.1101/061481.
39. Kadir, S. N., Goodman, D. F. M. & Harris, K. D. High-Dimensional Cluster Analysis with the Masked EM Algorithm. *Neural Computation* **26**, 2379–2394 (2014).
40. Petersen, P. C., Siegle, J. H., Steinmetz, N. A., Mahallati, S. & Buzsáki, G. CellExplorer: A framework for visualizing and characterizing single neurons. *Neuron* **109**, 3594-3608.e2 (2021).